# 3D SPATIAL FOCAL CONTROL BY ARRAYED OPTOFLUIDIC PRISMS

Cheng-Hsun Lee, Yeonwoo Lee, and Sung-Yong Park\*

Department of Mechanical Engineering, San Diego State University, San Diego, CA, USA

# **ABSTRACT**

A new 3D focal control system composed of arrayed optofluidic prisms is presented. Through dynamic control of the fluid-fluid interface via electrowetting, incoming rays are spatially steered to achieve 3D focal control. Analytical study identifies the prism angle required to obtain a focal point at  $P_{\text{focal}} = (f_x, f_y, f_z)$  located in 3D space. Experimentally, an arrayed system has demonstrated its 3D focal tunability along  $0 \le f_x \le 30$ ,  $0 \le f_y \le 30$ , and  $500 \le f_z \le \infty$  in millimeters. This new lens capability for 3D focal control can be potentially used for tracking eye movement for smart displays, or solar tracking for smart compact concentrated photovoltaic systems.

### **KEYWORDS**

Electrowetting, liquid prism, optofluidics, focal length, arrayed system

# INTRODUCTION

Conventional solid-type optical devices typically require bulky and complex moving parts for rapid and spatial beam steering. These additional mechanical components make the systems bulky, costly, and complex, and lack their agility [1]. To address the issue, recent studies have demonstrated rapid and wide-angle beam steering using an electrowetting-based microfluidic technology [2, 3]. Electrowetting has been widely developed as an effective means for small-scale liquid handling due to the dominance of surface tension forces over body forces in micro/meso scales [4, 5]. It enables to control the shape and position of a liquid interface for effective light control through the applications of bias voltages instead of mechanical inputs. A liquid lens is one common example of the optofluidic devices controlled by the electrowetting principle [6, 7]. Smooth surface of a liquid drop allows to function it as an optical lens where electrowetting actively controls its curvature for focal tuning of a lens. Another type of optofluidic device relying on electrowetting is the liquid prism for beam steering [8, 9]. A prism is filled with two immiscible liquids with different refractive indices. The electrowetting effect controls the prism apex angle which in turn steers beam pathway. However, all previous works [2, 3, 6-8] was limited to linear tuning focal control.

This study presents a new 3D focal control system composed of  $n \times n$  arrayed optofluidic prisms. Dynamic control of the fluidic interface via electrowetting enables convergence of incoming light rays on a focal point located in 3D space. An advantage of such an optofluidic system is that light control can be achieved instantaneously without the need for bulky and complicated mechanical moving parts. Analytical study predicts the prism angle required to achieve 3D focal tunability of the optofluidic system. Experimental studies have further demonstrated 3D focal tunability of the system by simultaneously performing light focusing along lateral, longitudinal, and axial directions as

much as  $\leq f_x \leq 30$ ,  $0 \leq f_y \leq 30$ , and  $500 \leq f_z \leq \infty$  in millimeters. Such 3D focal tunability opens up a door to the development of tunable, compact optical devices for crucial applications such as tracking eye movement for smart displays or solar tracking for smart compact concentrated photovoltaic systems.

# AN ARRAYED OPTOFLUIDIC PRISM SYSTEM FOR 3D FOCAL CONTROL

Figure 1(a) shows a schematic of the optofluidic beam steering system that enables spatial focal control of incoming rays in 3D space. It consists of  $n \times n$  arrayed liquid prisms filled with two immiscible liquids such as water and oil. A curved meniscus is formed at the interface with an initial contact angle of  $\theta_0$  on the sidewall surface of the prism. When bias voltages are applied to the prism's sidewalls, the electrowetting effect is induced to modify the surface tension force and results in the contact angle changes. Such contact angle modifications enable to have a straight profile of the interface with an apex angle  $(\varphi)$  of the prism (Figure 1b). With the two liquids whose refractive indices are different each other, incoming light can be manipulated for 3D beam steering without any mechanical moving components like gimbaled mirrors. This beam steering performance has been demonstrated in previous studies using an electrowetting-driven liquid prism [2, 3, 6-8]. However, all previous demonstrations were limited to linear optical tuning. To achieve 3D focal control, our study herein proposes an  $n \times n$  arrayed form of a single prism module. Each prism of the arrayed optofluidic system is individually controlled to provide its own prism angle  $(\varphi)$  using the electrowetting principle.

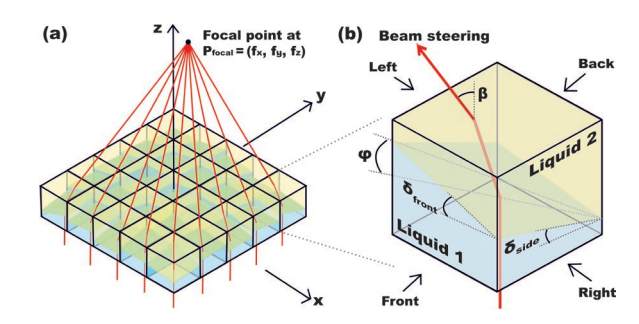


Figure 1: (a) An  $n \times n$  arrayed form of the optofluidic prism system for 3D focal control and (b) an enlarged image of a single prism module filled with two immiscible liquids. A liquid prism is controlled via electrowetting to have a straight profile of the fluidic interface with an apex angle  $(\varphi)$  of the prism. Due to the refractive index differences  $(n_1 \neq n_2 \neq n_{air})$  of each medium, an incoming light beam is dynamically manipulated at the interface for 3D beam steering. By symmetrically or asymmetrically controlling individual prisms in the array system, light focusing can be achieved in 3D free space, truly offering a new lens capability for 3D focal control without the need of bulky and complex mechanical moving components.

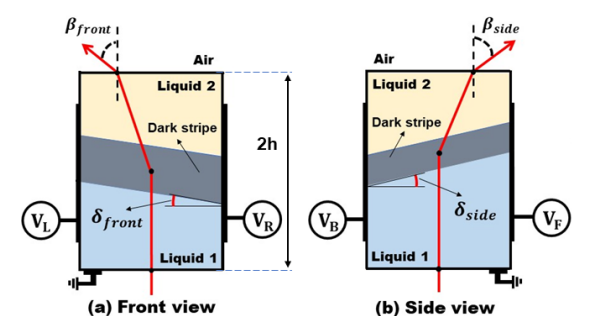


Figure 2: (a) Front and (b) side views of a single prism at an arbitrary location of P(x, y, 0). When bias voltages  $(V_L, V_R, V_F, \text{ and } V_B)$  are applied to four sidewalls of the prism, the fluidic interface is controlled via electrowetting to have the straight profile with the prism angle  $(\varphi)$ . The tilted angles  $(\delta_{front}$  and  $\delta_{side})$  of a dark stripe simply observed in the front and side views can be used to confirm the prism angle  $(\varphi)$  controlled in 3D space.

Consequently, incoming light can be spatially steered for light focusing on a focal point that is located at  $P_{\text{focal}}(f_x, f_y, f_z)$  in 3D space. This 3D optical tunability enables to dynamically modulate the lens' power that couldn't be implemented by solid-type optics without bulky and complex mechanical moving components.

# PRISM ANGLE CONTROL IN 3D

**Performance analysis:** To control the fluidic interface in 3D via electrowetting, bias voltages  $(V_F, V_B, V_L, \text{ and } V_R)$  are separately applied at four sidewalls of the prism, respectively. The surface tension modification results in the contact angle changes on each sidewall of the prism. The resultant contact angles  $(\theta_F, \theta_B, \theta_L, \text{ and } \theta_R)$  modulated from an initial angle  $\theta_0$  on four sidewalls are mathematically estimated as using the Young-Lippmann equation [2, 3]:

$$\cos \theta_F = \cos \theta_0 + \frac{1}{2\gamma} c V_F^2, \quad \cos \theta_B = \cos \theta_0 + \frac{1}{2\gamma} c V_B^2$$

$$\cos \theta_L = \cos \theta_0 + \frac{1}{2\gamma} c V_L^2, \quad \cos \theta_R = \cos \theta_0 + \frac{1}{2\gamma} c V_R^2$$
(1)

where c is the specific capacitance of a dielectric layer and  $\gamma$  is the interfacial tension between two liquids. An incoming ray perpendicularly projected from the bottom can be refracted as much as the prism angle ( $\varphi$ ) at the interfaces due to the refractive index difference ( $n_1 \neq n_2 \neq n_{\rm air}$ ) between two media. Using the geometrical relations and Snell's law at the interfaces, the beam steering angle  $\beta$  of the ray as it exits the prism can be also estimated as:

$$\beta = \sin^{-1} \left( n_1 \sin \varphi \cos \varphi - n_2 \sin \varphi \sqrt{1 - \left( \frac{n_1}{n_2} \sin \varphi \right)^2} \right)$$
 (2)

which is expressed as a function of the refractive indices  $(n_1 \text{ and } n_2)$  of the two liquids and the prism angle  $(\varphi)$ .

Since the fluidic interface is spatially modulated to have a straight profile, it is difficult to recognize the prism angle  $(\varphi)$  controlled in 3D space. To simply estimate  $\varphi$ , we have instead used two observable parameters shown in the front and side views. Figure. 2 shows schematic illustrations visualized on the front and side views of the prism positioned at an arbitrary location of  $P_C(x, y, 0)$  when the fluidic interface is spatially modulated with the prism angle  $(\varphi)$ . The prism has its height of 2h. Due to less light transmission, the 3D manipulated interface can be visualized as a dark stripe in the front and side views. This dark stripe is characterized with the tilted angles  $(\delta_{\text{front}}$  and  $\delta_{\text{side}})$  simply observed from experiments, as presented in Fig. 2(a) and (b). To have a straight profile (i.e.,  $\theta_L + \theta_R = 180^{\circ}$  and  $\theta_F + \theta_B = 180^{\circ}$ ) of the interface with the prism angle  $(\varphi)$  in 3D, the contact angles are modulated in such a manner that fulfils the following relations:

$$\delta_{front} = \theta_L - 90^{\circ} \text{ when } \theta_L \ge 90^{\circ} \ge \theta_R$$

$$\delta_{side} = \theta_F - 90^{\circ} \text{ when } \theta_F \ge 90^{\circ} \ge \theta_B$$
(3)

These two observable parameters ( $\delta_{\text{front}}$  and  $\delta_{\text{side}}$ ) obtained from experiments can be expressed as a function of  $\varphi$  and  $\omega$  using the geometrical relations:

$$\tan \delta_{front} = \tan \varphi \cos \omega$$

$$\tan \delta_{side} = \tan \varphi \sin \omega$$
(4)

where  $\omega$  indicates the azimuth angle of the ray's pathway from an x axis. With the given information on the prism location at  $P_C(x, y, 0)$  and the desired focal point  $P_{\text{focal}}(f_x, f_y, f_z)$  to be achieved by a liquid prism, the value of  $\omega$  can be estimated as:

$$\omega = \tan^{-1} \left( \frac{f_y - y}{f_x - x} \right) \tag{5}$$

Thus, Eq. (4) informs us that the two observable parameters,  $\delta_{\text{front}}$  and  $\delta_{\text{side}}$ , can be simply used to ensure the magnitude of the prism angle  $(\varphi)$  achieved. When combing Eq. (1), (3), and (4), one can know the bias voltages required to obtain the prism angle  $(\varphi)$  in 3D. With the given values of  $\omega$  and  $\varphi$ , we can further express the direction of the fluidic interface in a unit vector  $(\hat{n})$  normal to the surface of the interface as:

$$\hat{n} = \begin{bmatrix} -\sin\varphi\cos\omega \\ -\sin\varphi\sin\omega \\ \cos\varphi \end{bmatrix} \tag{6}$$

**Experimental demonstrations:** When electric potentials  $(V_{\rm F}=107~{\rm V},\,V_{\rm B}=51~{\rm V},\,V_{\rm L}=106~{\rm V},\,{\rm and}\,V_{\rm R}=51~{\rm V})$  were applied to four sidewalls of the prism, the fluidic interface was modulated to have a straight profile with the prism angle  $(\varphi)$  in 3D. Fig. 3(a) and Fig.3(b) shows the front and side views of the prism experimentally obtained, where the interface was visualized as a dark stripe that is characterized with a non-zero tilted angle of  $\delta_{\rm front}=-7^{\circ}$  in the front view, while  $\delta_{\rm side}=7^{\circ}$  in the side view, respectively. For an illustration purpose, let's assume that a prism is located on a 45° diagonal direction and desired to have its focal point along a z-axis for axial focal control

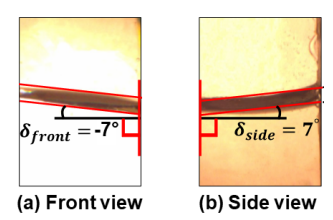


Figure 3: Experimental demonstrations of the fluid-fluid interface control in 3D via electrowetting. Control of the fluidic interface in 3D is visualized as a dark stripe with the tilted angles ( $\delta_{front} = \delta_{side} = 7^{\circ}$ ) shown in (a) the front and (b) side views, respectively. These observation parameters can be simply used to confirm the prism angle at  $\varphi = 10^{\circ}$  achieved.

(i.e.,  $\omega = 45^{\circ}$ ,  $f_x = f_y = 0$ , and  $f_z \neq 0$ ). Simply using these two observation parameters of tilted angles ( $\delta_{\text{front}}$  and  $\delta_{\text{side}}$ ) and the information on the prism location and desired focal point, experimental results in Fig. 3 confirmed that the fluid-fluid interface was successfully modulated via electrowetting to have a straight profile with the prism angle at  $\varphi = -10^{\circ}$  and the unit normal vector  $\hat{n} = \begin{bmatrix} 0.1228, & 0.1228, & 0.9848 \end{bmatrix}$  to indicate the direction of the fluidic interface.

# AXIAL FOCAL CONTROL

**Performance analysis:** This section discusses about the prism angle requirement to achieve axial focal control along the central lens axis (i.e., the z axis). Through symmetrical modulation of individual prisms, all incoming rays can be steered to be converged at a single point of  $P_{\text{focal}}$   $(0, 0, f_z)$  on the z axis. A key consideration is to find  $f_z$  as a function of  $\varphi$  and  $\omega$  for the prism located at  $P(r, \theta, 0)$ , where  $r = \sqrt{x^2 + y^2}$  is a radial distance of  $P_C$  from an origin and  $\theta = \tan^{-1}(y/x)$  is an azimuth angle from an x axis. For axial focal control,  $f_x = f_y = 0$ . Thus, it is given that  $\omega = \theta$ . Then,  $f_z$  can be written as:

$$f_z = (r - a)\cot \beta + h \tag{7}$$

where *a* is denoted as the distance between the intersection point of the ray on the top surface of the prism and the vertical line extended from the prism center, which can be estimated as:

$$a = h \tan \left\{ \sin^{-1} \left( \frac{\sin \beta}{n_2} \right) \right\}$$
 (8)

By substituting Eq. (2) and (8) into Eq. (7), the focal point  $f_z$  on a z axis can be plotted as a function of  $\varphi$  for various prism locations of r along a radial direction, which is shown in Fig. 4. For this analytical study, a liquid prism is assumed to be filled with binary liquids of 1-bromonaphthalene (1-BN) as a high-refractive-index oil  $(n_1 = 1.65)$  and water  $(n_2 = 1.33)$ , and to have its height 2h = 25 mm, which will be the same conditions of our succeeding experimental tests. Fig. 4 provides critical information on the prism angle  $\varphi$  required for the prism positioned at  $P_C$   $(r, \theta, 0)$  to achieve the ray focusing on a

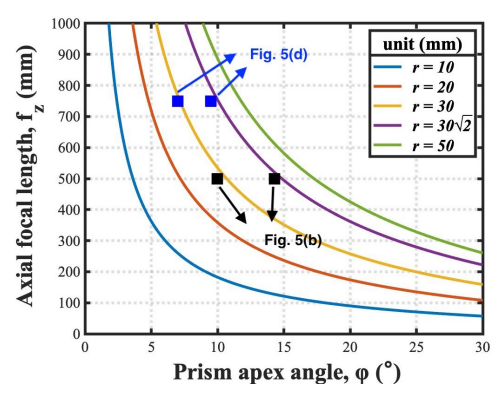


Figure 4: Axial focal tunability of the arrayed optofluidic system. An axial focal length  $f_z$  on a z axis is presented as a function of the prism angle  $\varphi$  for various prism distances of r in a radial direction from an origin. At higher prism angles, more beam steering and thus shorter focal lengths can be achieved, resulting in higher lens power. Four data points added in the graph indicate the axial focal length  $f_z$  obtained from the experimental tests shown in Fig. 5 (b) and (c).

particular focal length  $f_z$  on a z axis for axial focal control. In general, a large apex angle is required for larger beam steering of incoming light, which leads to high lens power with a short focal length. Similarly, for the prisms with large r values (i.e., further from the origin), a high apex angle is required to compensate for their distance from the central axis.

For any other focal length  $f_z$  desired to be achieved, the required prism angles may be similarly determined for any prism location. For comparison with our analytical studies, four experimental data points are added to the graph for r = 30 and  $30\sqrt{2}$  mm to demonstrate the system's capability for axial focal control.

Experimental demonstrations: Figure 5 experimental results to demonstrate the lens' capability for axial focal control along a z axis. With the applications of bias voltages to the sidewalls of the three prisms, they were initially modulated to have all prism angles at  $\varphi_1 = \varphi_2 = \varphi_3$ =  $0^{\circ}$  and the normal directions to the fluid interfaces as  $\hat{n}_1 = \hat{n}_2 = \hat{n}_3 = \begin{bmatrix} 0, & 0, & 1 \end{bmatrix}$ . As a result, incoming laser beams pass through the three prisms in parallel with no light refraction at the interfaces. The top view as shown of Figure 5(a) indicates that the laser spots are located at the same positions as the prisms' locations at  $\varphi_1 = \varphi_2 = \varphi_3 = 0^\circ$ . This experimental result indicates that a focal point is said to be at infinity, i.e.,  $f_z = \infty$ . These three prisms were further controlled to achieve axial focal control. With the applications of the bias voltages, the three prisms were symmetrically controlled to have the prism angels at  $\varphi_1$  =  $10^{\circ}$ ,  $\varphi_2 = 10^{\circ}$ , and  $\varphi_3 = 14^{\circ}$  where the incoming laser beams were steered to be focused at  $P_{\text{focal}}(f_x, f_y, f_z) = (0, 0, 500)$ mm) for axial focal control on a z axis. Figure 5(b) shows the top view of the grid paper located at z = 50 cm where the three laser beams were focused on the origin. Figure 5(c) shows the convergence of three laser beams on the origin located at z = 75 cm to represent lower lens' power performance, when the prisms were controlled to have  $\varphi_1$ = 10°,  $\varphi_2 = 10^\circ$ , and  $\varphi_3 = 14^\circ$ .

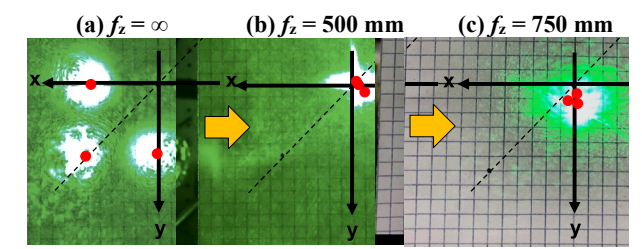


Figure 5: Experimental demonstrations of the focal control along an axial (z) direction by symmetrical prism control. (a) and (c) Three prisms are manipulated to have all prism angles at  $\varphi = 0^{\circ}$ . Then, the laser beams pass through each prism in parallel without beam steering, resulting an axial focal length located at  $f_z = \infty$  where the laser spots initially located at  $P_1$  (30, 0),  $P_2$  (0, 30), and  $P_3$  (30  $\sqrt{2}$ , 30  $\sqrt{2}$ ) in millimeters. After symmetrically controlling the prism angles, three laser beams are spontaneously steered to focus on the origin that is located at two different x-y planes of (b)  $f_z = 50$  cm and (d)  $f_z = 75$  cm. The test results demonstrated the lens capability for an axial focal control in z direction.

#### 3D FOCAL CONTROL

Figure 6 presents the focal tunability along both lateral and longitudinal directions by asymmetrically controlling the three prisms. With the prism angles of  $\varphi_1 = 6^{\circ}$ ,  $\varphi_2 = 9^{\circ}$ , and  $\varphi_3 = 8^{\circ}$  controlled via electrowetting, the arrayed system was able to show 3D focal tunability for which the focal point can be located at  $P_{\text{focal}}(f_x, f_y, f_z) = (20, 10, 500)$ in millimeters (Figure 6a). Figure 6(b) shows an experimental result of the focal point located at  $P_{\text{focal}}(f_x, f_y)$  $f_z$ ) = (30, 30, 500) in millimeters by controlling the prism angles of  $\varphi_1 = 10^{\circ}$ ,  $\varphi_2 = 10^{\circ}$ , and  $\varphi_3 = 0^{\circ}$ . Figure 6(c) presents 3D focal tunability to manipulate the focal point at  $P_{\text{focal}} = (30, 0, 500)$  in millimeters when  $\varphi_1 = 0^{\circ}$ ,  $\varphi_2 = 14^{\circ}$ , and  $\varphi_3 = 10^{\circ}$ . Experimental results presented in Figure 6 have successfully demonstrated 3D focal tunability of the arrayed optofluidic system by asymmetrical control of individual prisms.

#### **CONCLUSION**

To address the issue of conventional solid-type optical devices that typically require bulky and complex moving parts for rapid and spatial beam steering, recent studies have demonstrated wide-angle beam steering using optofluidic prism devices driven by electrowetting. However, the lens performance was limited to linear tuning, failing to fully exhibit the focal tunability in 3D space. This paper presents a new lens capability for 3D focal control, which couldn't be achieved by solid-type devices without bulky and complex mechanical moving parts. An optofluidic system consists of  $n \times n$  arrayed liquid prisms filled with two immiscible liquids such as water and oil. Dynamic control of the fluidic interface via electrowetting enables convergence of incoming light rays on a focal point located in 3D space. We have analytically studied to predict the prism angle required to achieve the desired focal location in 3D. Experimental studies have further demonstrated 3D focal tunability of the system by simultaneously performing light focusing along lateral,

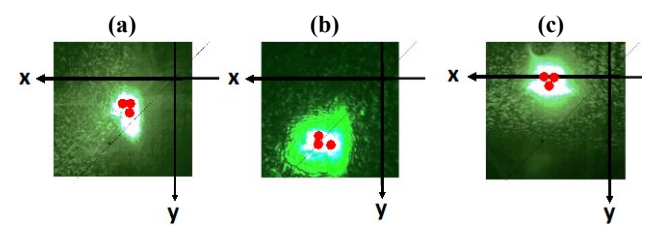


Figure 6: Experimental demonstrations of the 3D focal control along both lateral and longitudinal directions at  $f_z = 500$  mm through asymmetrical prism control. Light focusing of the three laser beams are variously tuned to have the focal points located at (a)  $f_x = 20$  and  $f_y = 10$ , (b)  $f_x = f_y = 30$ , and (c)  $f_x = 30$  and  $f_y = 0$  in millimeters, respectively.

longitudinal, and axial directions as much as  $\le f_x \le 30$ ,  $0 \le f_y \le 30$ , and  $500 \le f_z \le \infty$  in millimeters. This new lens capability for 3D focal control can be potentially used for smart tracking systems such as eye tracking for smart displays, or solar tracking.

#### **ACKNOWLEDGEMENTS**

This work was partially supported by the NSF CAREER Award (ECCS - 2046134), USA.

# REFERENCES

- [1] E. Arbabi, A. Arbabi, S. M. Kamali, Y. Horie, M. Faraji-Dana, and A. Faraon, "MEMS-tunable dielectric metasurface lens," *Nature Communications*, vol. 9, no. 1, p. 812, 2018.
- [2] C. Clement, S. K. Thio, and S.-Y. Park, "An optofluidic tunable Fresnel lens for spatial focal control based on electrowetting-on-dielectric (EWOD)," *Sensors and Actuators B: Chemical*, vol. 240, pp. 909-915, 2017.
- [3] C. E. Clement and S.-Y. Park, "High-performance beam steering using electrowetting-driven liquid prism fabricated by a simple dip-coating method," *Applied Physics Letters*, vol. 108, p. 191601, 2016.
- [4] A. R. Wheeler, "Putting Electrowetting to Work," *Science*, vol. 322, pp. 539 540, 2008.
- [5] S. K. Thio and S.-Y. Park, "A review of optoelectrowetting (OEW): from fundamentals to lab-on-a-smartphone (LOS) applications to environmental sensors," *Lab on a Chip,* vol. 22, no. 21, pp. 3987-4006, 2022.
- [6] B. W. Hendriks, S. Kuiper, M. J. VAN As, C. A. Renders, and T. W. Tukker, "Electrowetting-based variable-focus lens for miniature systems," *Optical Review*, vol. 12, no. 3, pp. 255-259, 2005.
- [7] S. Kuiper and B. H. W. Hendriks, "Variable-focus liquid lens for miniature cameras," *Applied Physics Letters*, vol. 85, p. 1128, 2004.
- [8] S. K. Thio, D. Jiang, and S.-Y. Park, "Electrowetting-driven solar indoor lighting (e-SIL): an optofluidic approach towards sustainable buildings," *Lab on a Chip*, vol. 18, pp. 1725-1735, 2018.
- [9] S. K. Thio, S. W. Bae, and S.-Y. Park, "Plasmonic nanoparticle-enhanced optoelectrowetting (OEW) for effective light-driven droplet manipulation," *Sensors and Actuators B: Chemical*, vol. 308, p. 127704, 2020.

### **CONTACT**

\*S.-Y. Park, tel: +1-619-594-2319; spark10@sdsu.edu